



Systematic determination of the optimized Zr content of $\text{Ba}(\text{Zr}_x\text{Ti}_{1-x})\text{O}_3$ with high dielectric constant at room temperature for high-voltage system application

Jandi Kim^{1,2} · Ji Hye Seo¹ · Sang Heun Lee^{1,2} · Myunghee Cho^{1,4} · Hun Kwak¹ · Ran Sae Cheon^{1,2} · Seungchan Cho³ · Sung Beom Cho^{5,6} · Minkee Kim⁷ · Yoon-Seok Lee⁸ · Yangdo Kim² · Moonhee Choi¹

Received: 24 July 2023 / Revised: 5 October 2023 / Accepted: 29 October 2023 / Published online: 19 January 2024
© The Author(s) 2024

Abstract

In this study, by replacing the B-site element in BaTiO_3 , a ferroelectric material, with an element with a larger ionic radius, a ferroelectric material with high permittivity at room temperature was synthesized. The powders were prepared by solid-state reaction to perform lattice substitution with Zr^{4+} (0.72 \AA), which has a larger ionic radius than Ti^{4+} (0.605 \AA). To perform effective solid-state reaction and better understand the correlation between variables, this study introduced a design of experiment (DOE) based on the orthogonal array (OA) method included in the PIAno software. By substituting 0.222 mol of Zr, which has a large ionic radius, the crystal structure was deformed through an effective diffuse phase transition (DPT), and this resulted in the largest improvement in permittivity at room temperature. In addition, the powder, which underwent solid-state reaction at 1300°C , formed the densest structure during sintering, which established the conditions for realizing the best dielectric properties. These results can be utilized as a key material for improving the properties of passive devices used in high-voltage industrial systems in societies undergoing the fourth industrial revolution.

Keywords Dielectric · MLCC · Barium zirconate titanate · Solid-state reaction

1 Introduction

BaTiO_3 is a ferroelectric ceramic material with a high relative permittivity at room temperature and an ABO_3 perovskite structure. Ba^{2+} ions and O^{2-} ions are located at the unit cell edges and face centers of BaTiO_3 , and Ti^{4+} ions

are detached at the unit lattice center to form a tetragonal structure at room temperature. When the A (Ba^{2+}) and B (Ti^{4+}) site elements of pure BaTiO_3 , which has a perovskite structure, are partially substituted with transition metals and rare-earth elements, the dielectric properties, electrical properties, reliability, and temperature properties are improved [1]. In particular, when Zr is added to

Jandi Kim and Ji Hye Seo are the co-primary authors.

✉ Yoon-Seok Lee
yoonseok@pknu.ac.kr

✉ Yangdo Kim
yangdo@pusan.ac.kr

✉ Moonhee Choi
moonhee77.choi@kicet.re.kr

¹ Electronic Convergence Division, Korea Institute of Ceramic Engineering & Technology, 101, Soho-Ro, Jinju 52851, South Korea

² School of Materials Science and Engineering, Pusan National University, Busan 46241, South Korea

³ Composites Research Division, Korea Institute of Materials Science, Changwon 51508, South Korea

⁴ School of Materials Science and Engineering, Gyeongsang National University, Jinju, Gyeongnam 52828, South Korea

⁵ Department of Materials Science and Engineering, Ajou University, Suwon 16499, South Korea

⁶ Department of Energy Systems Research, Ajou University, Suwon 16499, South Korea

⁷ R&D Center, Samhwa Capacitor, 227, Gyeonggidong-Ro, Yongin 17118, South Korea

⁸ Department of Materials System Engineering, Pukyong National University, Busan 48547, South Korea

the B-site, the material becomes chemically stable, and good dielectric properties can be achieved [2, 3]. Moreover, substitution with Zr^{4+} (0.72 Å), which has a larger ionic radius than Ti^{4+} (0.605 Å), causes lattice expansion, which increases the dielectric constant and reduces the Curie temperature (T_c) [4]. Due to these phenomena, compositionally optimized Ba–Zr–TiO₃ dielectric material is used in capacitors that are capable of providing excellent dielectric properties [5, 6]. Currently, electronics in internal combustion engine automobiles are rapidly developing and becoming more high voltage, and the industry is switching from 12- to 24-V electrical systems to 48-V systems [7, 8]. In addition, eco-friendly electrical vehicles are adding various features, such as Direct Current–Direct Current (DC–DC) converters, inverters, advanced driver assistance systems (ADAS), engine control units (ECU), and autonomous driving systems, which are increasing the demand for capacitors that can easily drive high-voltage systems of more than 400 V [9–11].

Therefore, in this study, we investigated dielectric materials that can realize high permittivity at room temperature for high-voltage systems. In particular, we studied the substitution of Zr ions to induce lattice expansion at the B-site in the perovskite structure. To develop an optimal Ba(Zr_xTi_{1-x})O₃ composition for providing excellent dielectric properties at room temperature, a design of experiment (DOE) based on the orthogonal array (OA) method [12] was applied to effectively conduct the composition development study. These are the applications of statistics aimed at designing efficient experimental methods and properly analyzing results. These were applied to plan how to conduct the experiment to obtain maximum information with the minimum number of experiments. These were able to determine the optimal experimental conditions and shorten the composition development cycle. In addition, based on the results of each experimental condition, we identified the correlation between dielectric properties, microstructures, crystal structures, and temperature properties.

2 Experiment

2.1 Precursors

In this study, BaCO₃ with a Brunauer, Emmett, Teller (BET) size of 11.2 m²/g was used as the A-site element in solid-state reaction, TiO₂ with a BET size of 8.6 m²/g was used as the B-site element, and ZrO₂ with a BET size of 48.6 m²/g was used as the B-site substitution element for controlling properties (Fig. 1a~c).

2.2 Solid-state reaction

To perform experiments on the composition of Ba(Zr_xTi_{1-x})O₃, which has a high permittivity at room temperature, powders were prepared via solid-state reaction. The procedure for solid-state reaction is as follows: (1) precursor dispersion, (2) mixing for solid-state reaction, and (3) high-temperature heat treatment of the mixed powders. During synthesis, the molar ratio of the A-site element, BaCO₃, was fixed at 1 mol, and various molar ratio combinations of ZrO₂ and TiO₂ were used at the B-site to form the Ba(Zr_xTi_{1-x})O₃ mixture. The various mixtures were each held at 1000–1400 °C for 4 h by increasing the temperature at a rate of 1 °C/min to obtain a solid-state-reacted powder after furnace cooling (Fig. 2).

2.3 Properties evaluation

To observe the dielectric properties and microstructures of each of the powders, uniaxial pressing was performed at 127 MPa. The pressed samples were put through a firing process in an air condition at a temperature of 1000–1300 °C for 2 h to produce sintered samples. The sintered samples' dielectric property behaviors were analyzed and evaluated according to their (1) sintered densities, (2) dielectric properties, (3) microstructures, and (4) dielectric properties behaviors according to temperature changes. Furthermore, to identify the causes of changes in each sintered material's properties, the solid phase synthesized powders were analyzed and

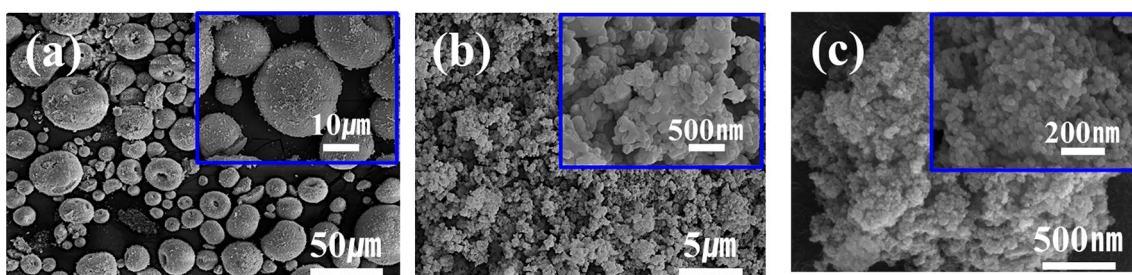


Fig. 1 Precursors for Ba(Zr_xTi_{1-x})O₃ solid-state reaction **a** BaCO₃, **b** TiO₂, and **c** ZrO₂

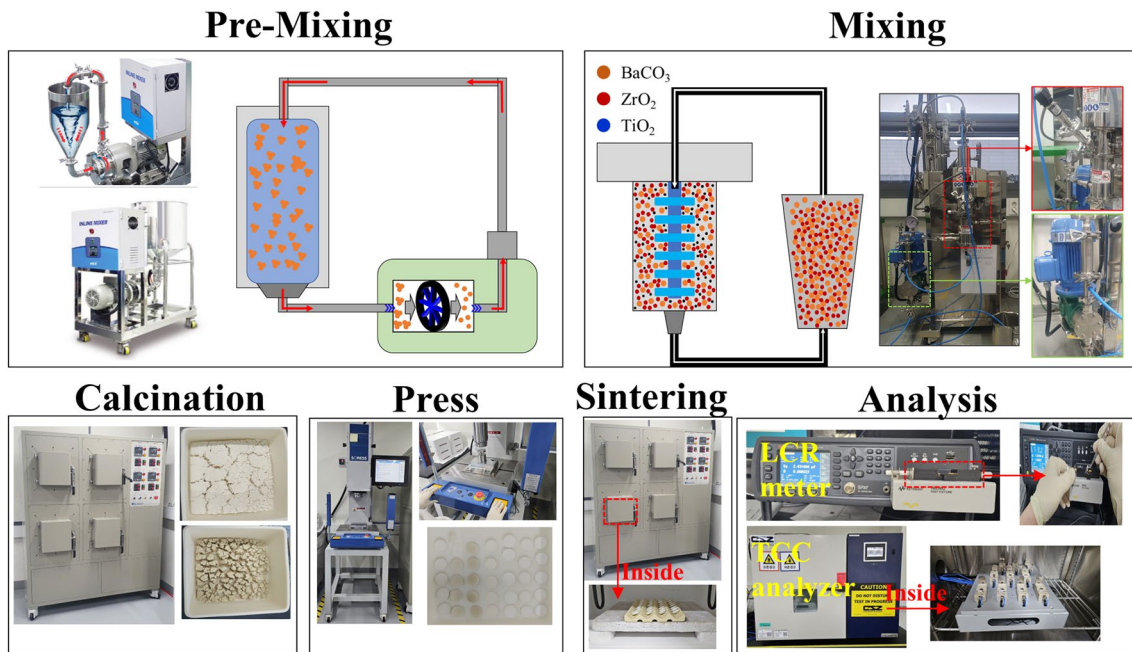


Fig. 2 $\text{Ba}(\text{Zr}_x\text{Ti}_{1-x})\text{O}_3$ powder solid-state reaction and evaluation equipment

evaluated by performing (5) crystal analysis, and (6) microstructure analysis in parallel.

3 Results and discussion

To reduce the number of experiments and better understand the correlation between variables, this study used a DOE based on the OA method included in the PIAno software. To explore the composition variables more closely, 10 levels were considered, and five levels were considered for the process variables. Here, the saturated points were determined using a full quadratic polynomial model among the experiment variables, and the corresponding number of

experiments (sampling points) was set to 60, which is more than 1.5 times the number of saturated points, $L_{60}(10^1 \times 5^3)$. Moreover, additional experimental variables were further tested using the Argument Latic Hypercube Design (ALHD) method to maximize the orthogonality between the existing sampling points (Fig. 3).

To optimize the composition conditions for $\text{Ba}(\text{Zr}_x\text{Ti}_{1-x})\text{O}_3$, which provides excellent dielectric properties at room temperature, solid-state reaction was performed after partially substituting the B-site element Ti with Zr. Mixing and solid-state reaction were performed after primary dispersion of each starting material, which allowed the solid-state reaction to proceed easily [13]. To replace the B-site element Ti, 0.055–0.222 mol of Zr was added in controlled amounts

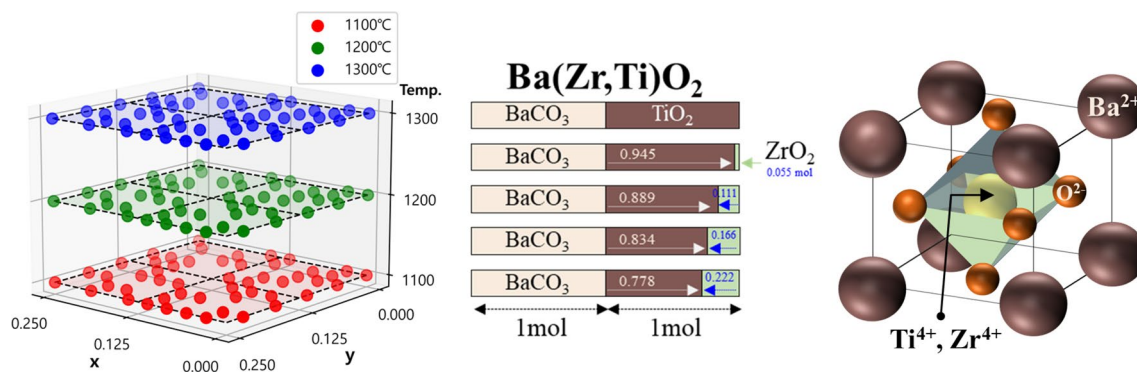


Fig. 3 Solid-state reaction composition design experiment for synthesizing $\text{Ba}(\text{Zr}_x\text{Ti}_{1-x})\text{O}_3$ powder

to create the mixtures. Subsequently, a heat treatment was performed for 4 h at 1000 °C to synthesize the ceramic powders. The structures of the synthesized powders were analyzed, and the results showed that no major changes in the crystal structure were observed when 0.055 mol of Zr was substituted in the B site. However, when 0.111 mol or more was added, it was found that the cubic structure of BaZrO_3 and $\text{BaZr}_{0.25}\text{Ti}_{0.75}\text{O}_3$ and the orthorhombic structure of $\text{BaZr}_{0.05}\text{Ti}_{0.95}\text{O}_3$ crystal phases were mixed (Fig. 4a). When calcination was performed after heating to a temperature of 1100 °C, the results showed that the Ba-Zr-TiO₃ crystal phases with cubic and orthorhombic structures mixed only at a substitution level of 0.222 mol (Fig. 4b). When calcination was performed at 1200 and 1300 °C, it was found that the material was calcinated into cubic structure of $\text{BaZr}_{0.25}\text{Ti}_{0.75}\text{O}_3$ powder in all mixing conditions (Fig. 4c, d).

In this study, we analyzed the lattice parameter crystal lattice changes that occurred along the unit cell a and c axes of the powders that were synthesized under various conditions.

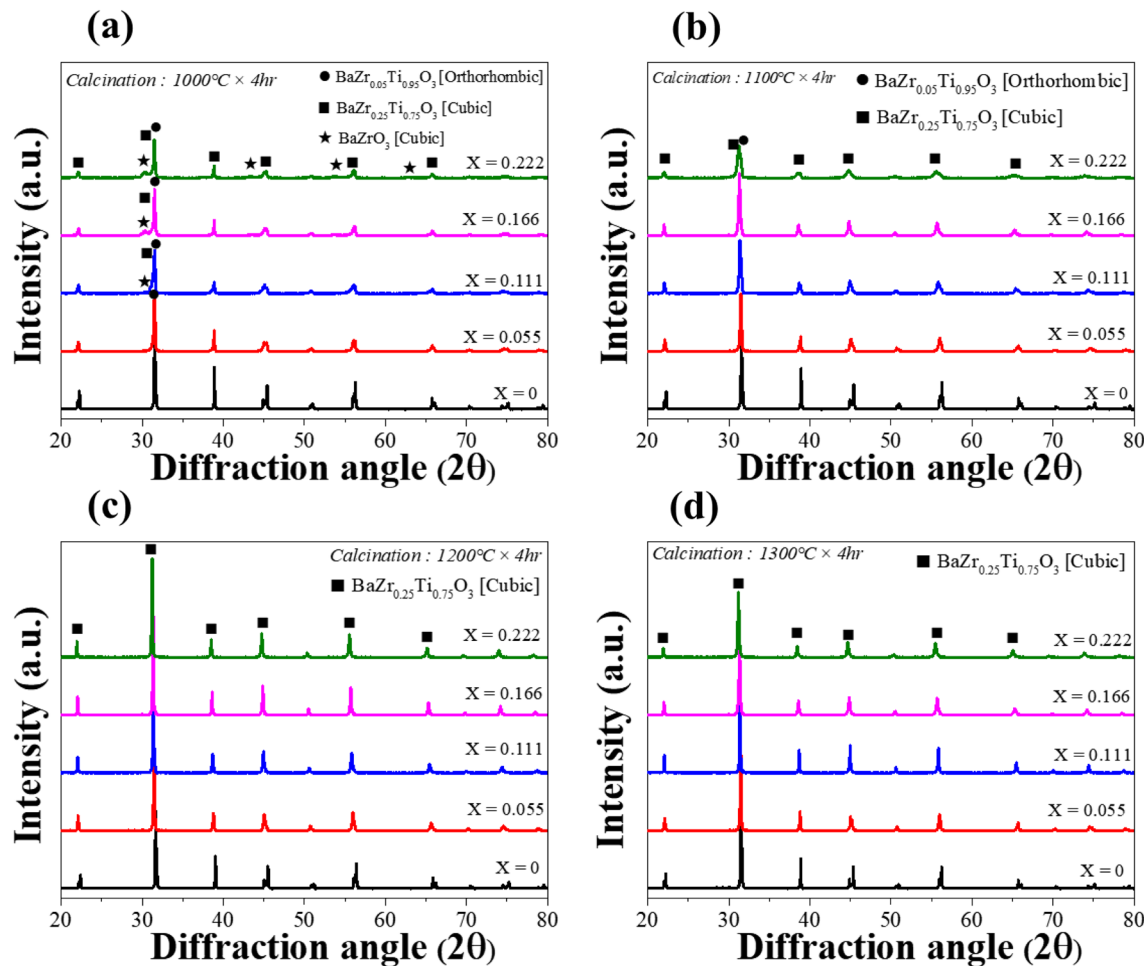
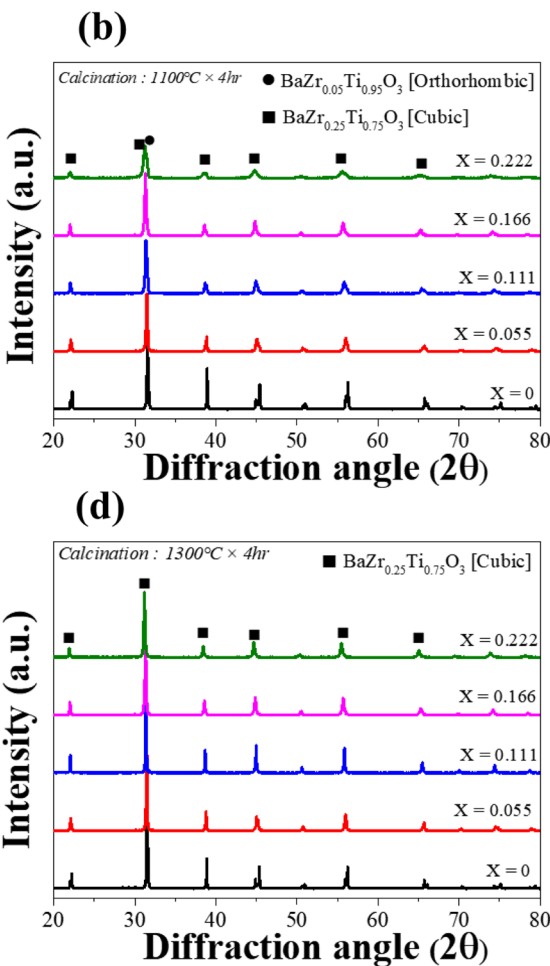


Fig. 4 Crystal structure analysis results for solid-state-reacted powder under various calcination temperature conditions. **a** Calcination temperature of 1000 °C×4 h **b** Calcination temperature of 1100 °C×4 h

At a calcination temperature of 1000 °C, no crystal lattice changes were observed. However, at a calcination temperature of 1100 °C, crystal lattice changes were observed, and increases in the crystal lattice were observed as the temperature was increased to 1200 and 1300 °C and the amount of added Zr was increased (Fig. 5a–d). This is because the B-site lattice substitution amount increases according to the increase in the amount of Zr additive, which has a large ionic radius. As the Zr^{4+} ions, which have a larger ionic radius than Ti^{4+} , replace the B-site element Ti^{4+} ions, the oxygen ions of the oxygen octahedron containing the Zr^{4+} ions are pushed in the <100> direction. The space decreases in the <100> direction of the Ti^{4+} ions located in the adjacent oxygen octahedron, and a diffuse phase transition (DPT) phenomenon occurs, suppressing the Ti^{4+} ion oscillation. As a result of the DPT, the tetragonal BaTiO_3 ferroelectric phase changes to a cubic state [14–17].

We observed the synthesized microstructures of the powders calcinated at a temperature of 1000 °C, in which the



c Calcination temperature of 1200 °C×4 h, and **d** Calcination temperature of 1300 °C×4 h

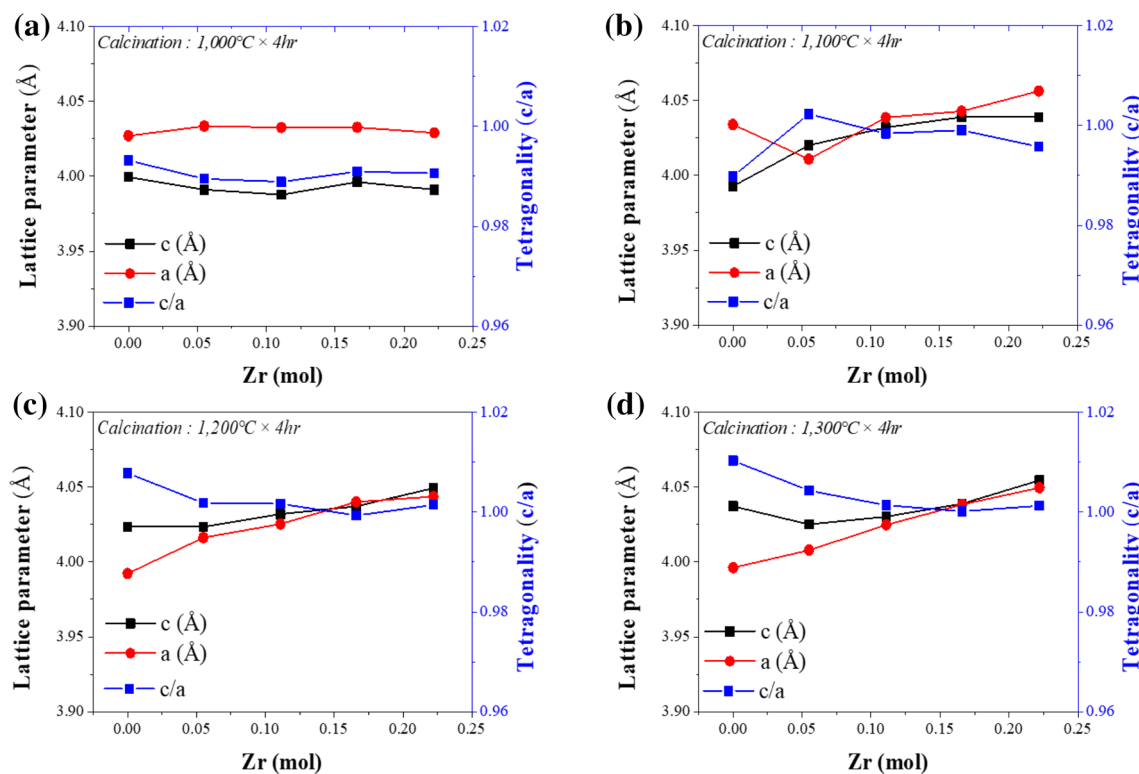


Fig. 5 Results of analyzing the lattice parameters and tetragonality of the $\text{Ba}(\text{Zr}_x\text{Ti}_{1-x})\text{O}_3$ powder calcinated with 0–0.222 mol of Zr additive (calcination at **a** 1000 °C, **b** 1100 °C, **c** 1,200 °C, and **d** 1300 °C)

Ba–Zr–TiO₃ phase and the BaZrO₃ phase with cubic and orthorhombic crystal structures were mixed. The results of the microstructure analysis showed that grain growth did not occur, because there was not enough thermal energy to allow the solid-state reaction to proceed sufficiently (Fig. 6a–f). Based on the results of the crystal analysis and the microstructure analysis, it was found that the addition of 0.166 and 0.222 mol of Zr at 1000 °C did not provide suitable synthesis temperature conditions for BZT synthesis.

The powder microstructure was observed after calcinating the $\text{Ba}(\text{Zr}_x\text{Ti}_{1-x})\text{O}_3$ mixture at 1200 °C for 4 h, and the results showed that grain growth occurred throughout the material (Fig. 7a–f). When 0.055 and 0.111 mol of Zr was substituted, powders with some coarse-sized abnormal grain growths were observed (Fig. 7a–c). These powders with abnormal grain growth generally caused the deterioration of sintered density, permittivity, and loss properties after firing [18]. However, the powders that were synthesized by substituting 0.166 mol of Zr or more had uniform, fine-grained shapes with sizes of 424 and 277 nm (Fig. 7d, f).

Observing the microstructures of the powders synthesized at a calcination temperature of 1300 °C for 4 h showed that abnormal grain growth occurred when 0–0.111 mol of Zr was added. However, the XRD analysis and SEM microstructure analysis results showed that a uniform $\text{Ba}(\text{Zr}_x\text{Ti}_{1-x})$

O₃ powder with a size of roughly 400 nm was synthesized when 0.222 mol of Zr was added (Fig. 8a–f).

In general, when the Zr element is added to BaTiO₃, stress occurs due to B-site substitution by Zr⁴⁺ (0.72 Å), which has a larger ionic radius than Ti⁴⁺ (0.605 Å). Lattice substitution stress leads to interactions between solid-state reacted powders, and grain refinement occurs to control these interactions and alleviate the stress [19]. Therefore, grain refinement occurred when 0.166 and 0.222 mol of Zr was added. To find the firing conditions in which sintering densification occurs, sintered specimens were created by applying 127 MPa of pressure to powders synthesized through calcination at 1000 °C for 4 h. Next, property evaluations were performed after sintering at a firing temperature of 1000–1300 °C. At firing temperatures of 1000–1200 °C, the sintered density was found to be generally low, but at a temperature of 1300 °C, it was found that the sintered density value generally improved to 5.5 g/cc or more (Fig. 9).

In addition, it was found that the highest increase in permittivity and the lowest dielectric loss value occurred in the specimen that was calcinated with 0.222 mol of Zr added and sintered at 1300 °C (Fig. 10a, b).

Refinement to a size of 0.35 μm occurred when material composed of $\text{Ba}(\text{Zr}_{0.05}\text{Ti}_{0.995})\text{O}_3$ was calcinated at 1000 °C for 4 h and sintered at 1300 °C for 2 h (Fig. 11a–d).

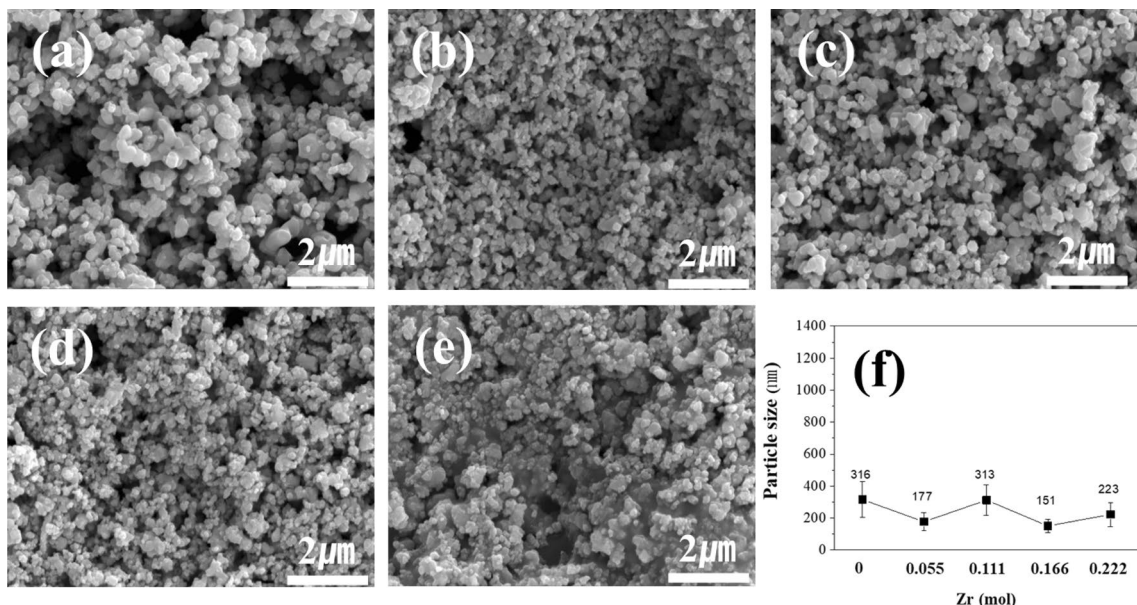


Fig. 6 Results of microstructure observations of powders that were solid state reacted with the $\text{Ba}(\text{Zr}_x\text{Ti}_{1-x})\text{O}_3$ mixture at $1000\text{ }^\circ\text{C}$ for 4 h
a $\text{Zr}=0$, b $\text{Zr}=0.055$, c $\text{Zr}=0.111$, d $\text{Zr}=0.166$, e $\text{Zr}=0.222$ mol, and f results of particle size distribution analysis of synthesized powders

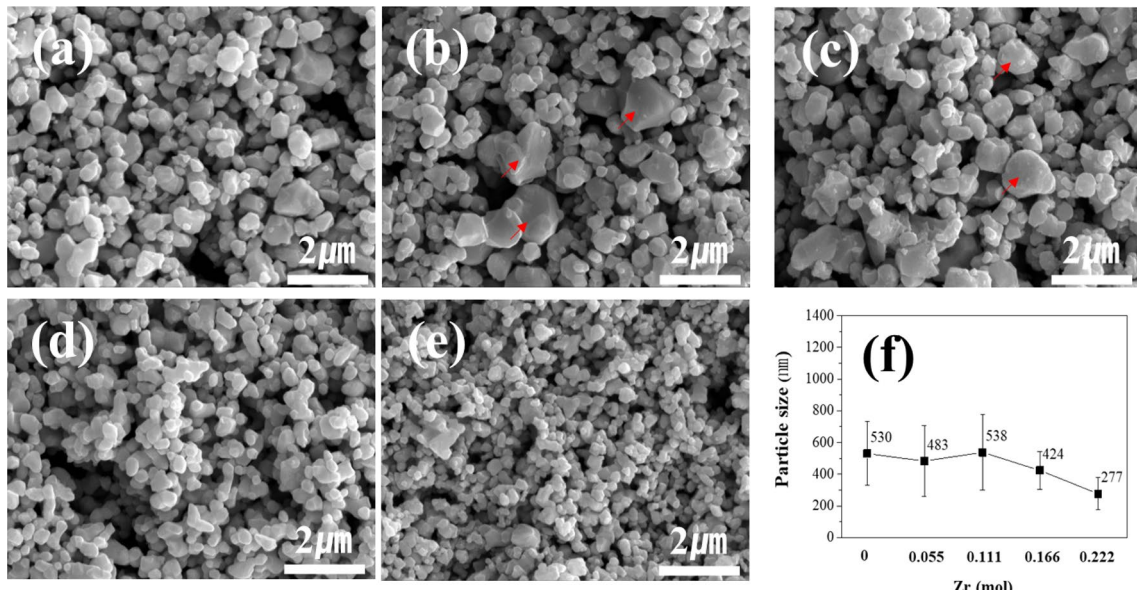


Fig. 7 Results of microstructure observations of powders that were solid state reacted with the $\text{Ba}(\text{Zr}_x\text{Ti}_{1-x})\text{O}_3$ mixture at $1,200\text{ }^\circ\text{C}$ for 4 h
a $\text{Zr}=0$, b $\text{Zr}=0.055$, c $\text{Zr}=0.111$, d $\text{Zr}=0.166$, e $\text{Zr}=0.222$ mol, and f results of particle size distribution analysis of synthesized powders

However, when the amount of Zr additive was increased to 0.222 mol, grain growth to a size of $1.13\text{ }\mu\text{m}$ was observed (Fig. 11e, f). As a result of this grain growth, permittivity increased [20–22]. In addition, the growth of coarse grains, as in the case of BaTiO_3 , considerably increases the probability of various flaws within the crystal, which act as defects that suppress domain motion. As a result, the dielectric

loss value increases considerably [23–25]. Moreover, even when the grain size is very small, parts with insufficient grain growth act to suppress domain motion, which increases dielectric loss, as shown in Fig. 11d [26]. However, when suitable grain growth occurs together with sintering densification, the permittivity and dielectric loss properties improve significantly.

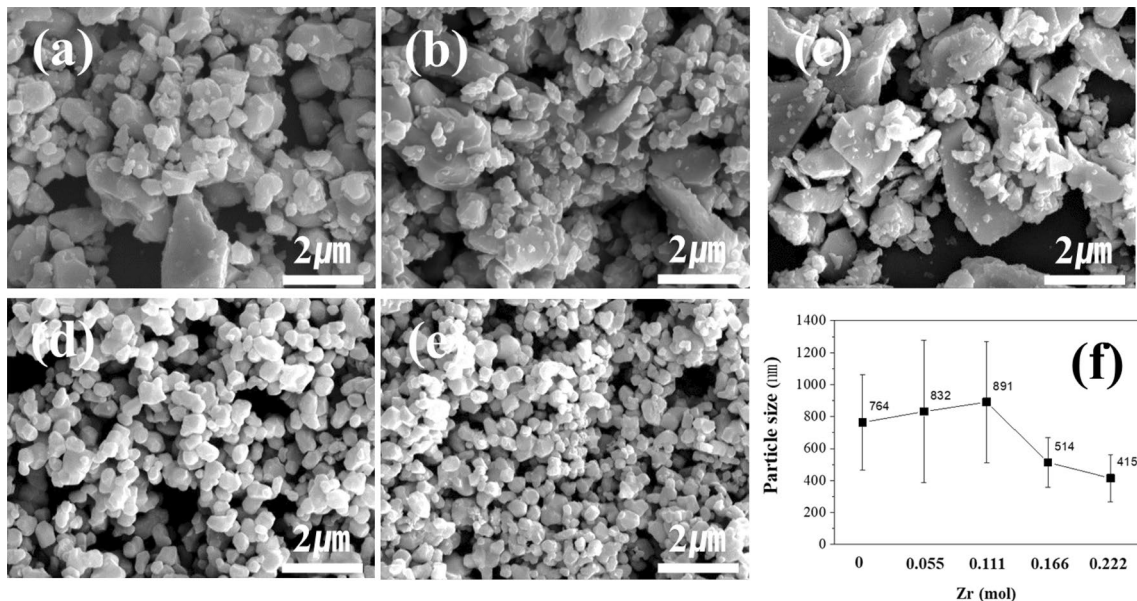


Fig. 8 Results of microstructure observations of powders that were solid state reacted with the $\text{Ba}(\text{Zr}_x\text{Ti}_{1-x})\text{O}_3$ mixture at $1300\text{ }^\circ\text{C}$ for 4 h
a $\text{Zr}=0$, b $\text{Zr}=0.055$, c $\text{Zr}=0.111$, d $\text{Zr}=0.166$, e $\text{Zr}=0.222$ mol, and f results of particle size distribution analysis of synthesized powders

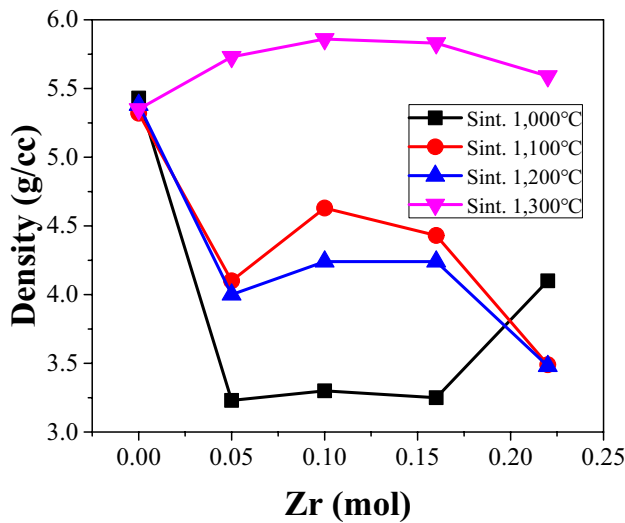


Fig. 9 Results of evaluating sintered densities of sintered specimens made from powder of $\text{Ba}(\text{Zr}_x\text{Ti}_{1-x})\text{O}_3$ mixture calcinated at $1000\text{ }^\circ\text{C}$ for 4 h ($1000\text{--}1300\text{ }^\circ\text{C} \times 2\text{ h}$)

In this study, we measured changes in permittivity according to temperature changes (-55–160°C) in the specimens calcinated at 1000 °C and sintered at 1300 °C after 0–0.222 mol of Zr additive was mixed at the B-site (Fig. 12a, b). The analysis results showed that the permittivity peak gradually moved toward room temperature as the B-site element Ti was partially replaced by Zr. When 0.166 mol of Zr was added, a high permittivity value was observed at around 55 °C, but at the room temperature interval, the permittivity

value was lower than when 0.222 mol was added. When Zr was added and B-site Ti substitution occurred, lattice expansion and lattice structure changes occurred due to the large ionic radius of Zr, which increases permittivity [27].

In addition, the results of the dielectric constant change rate with temperature change showed that the smallest change rate at room temperature was observed when 0.222 mol was added. Extremely high permittivity occurred around room temperature when 0.166 mol was added; furthermore, the permittivity change value was also very high. However, when 0.222 mol of Zr was added, the permittivity was extremely stable even when temperature changes occurred at room temperature.

To optimize the calcination conditions for the $\text{Ba}(\text{Zr}_{0.222}\text{Ti}_{0.778})\text{O}_3$ composition, the powders that were solid-state reacted within a calcination range of 1000–1400 °C were sintered at 1300 °C for 2 h, which is the optimal firing condition. The density values of the specimens that were sintered in each of the conditions were evaluated and analyzed, and the results showed that as the calcination temperature increased, the sintered density increased gradually. However, the sintered density decreased when sintering was performed on the powders calcinated at 1300 °C and above (Fig. 13).

In the case of the powder calcinated at 1300 °C, the microstructure observation results showed that the material was solid-state reacted into a fine and uniform powder with a size of 365 ± 86 nm (Fig. 14a). However, when the calcination temperature was increased to 1350 °C, abnormal grain growth was observed (Fig. 14b). At a calcination

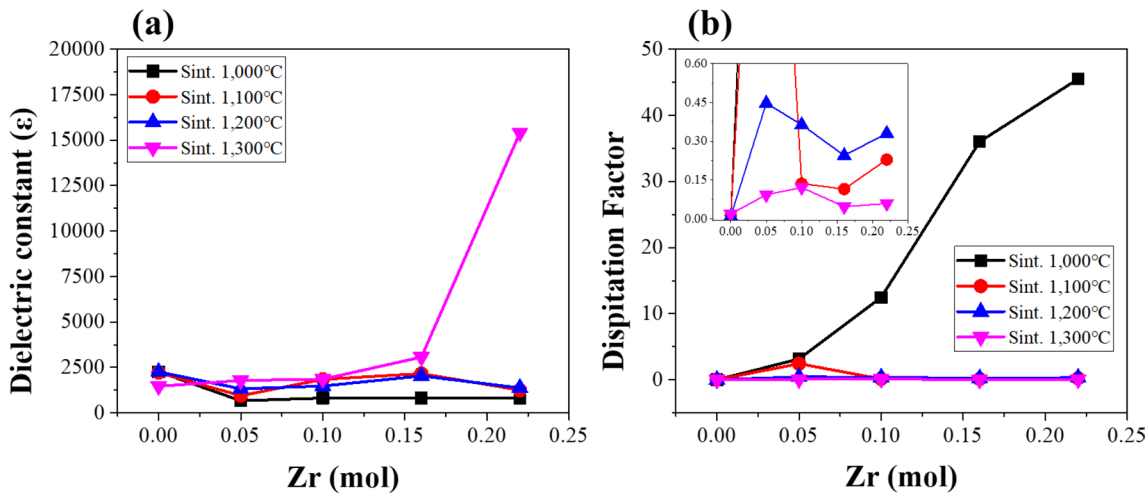


Fig. 10 Results of evaluating dielectric properties of specimens from $\text{Ba}(\text{Zr}_x\text{Ti}_{1-x})\text{O}_3$ mixture calcined at 1000 °C for 4 h and sintered at 1000–1300 °C for 2 h

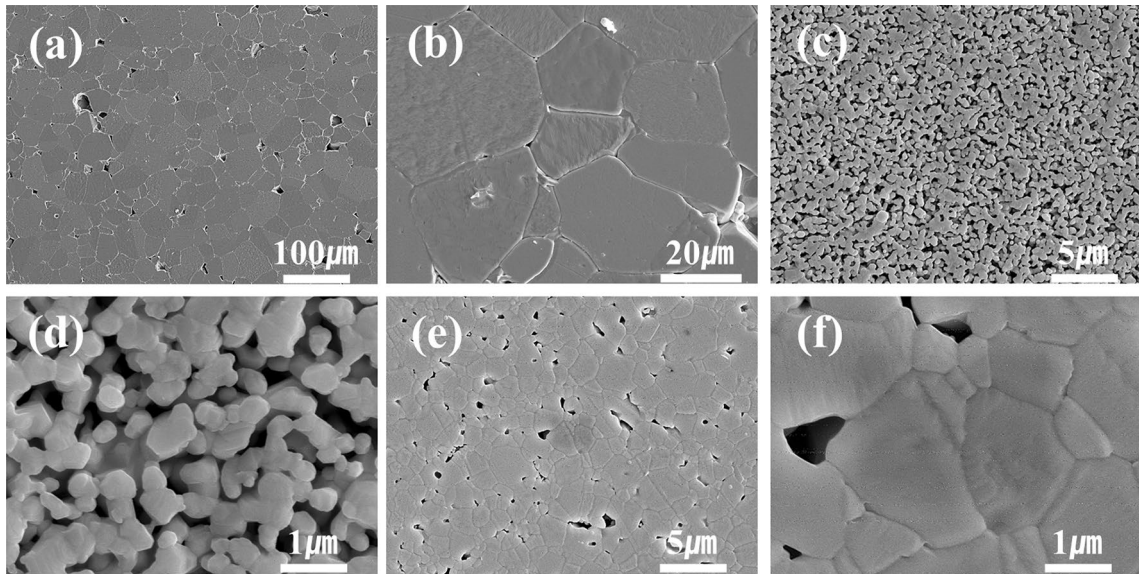


Fig. 11 Results of analyzing the fracture surface microstructure of specimens from $\text{Ba}(\text{Zr}_x\text{Ti}_{1-x})\text{O}_3$ mixture with 0, 0.055, and 0.222 mol of Zr calcinated at 1000 °C for 4 h and sintered at 1300 °C for 2 h (Zr added at **a**, **b** 0 mol, **c**, **d** 0.055 mol, and **e**, **f** 0.222 mol)

temperature of 1400 °C, abnormal grain growth occurred with overall coarse grain growth at 508 ± 233 nm, as shown in Fig. 14c. These powders with abnormal grain growth acted as the main cause of the decrease in sintered density.

The specimens that were created under the various conditions were used to evaluate dielectric properties, and the permittivity measurement results showed that when the calcination temperature was increased to 1000–1300 °C, the permittivity values increased continuously. However, the permittivity values started to decrease, starting at a calcination temperature of 1350 °C at which abnormal grain growth occurred, and the sintered density decreased. Moreover, the

dielectric loss increased rapidly in the powders that were calcinated at 1350 °C and above (Fig. 15a, b).

The fracture surface microstructures of the specimens that were sintered under various conditions were observed, and the results showed densely filled microstructures of around 27 μm when using the powder that was calcinated at 1300 °C (Fig. 16a, b), showing the best-sintered density and permittivity values. However, when firing was performed using the powder that was calcinated at 1350 °C, where many abnormal grain growths were present, defects such as large grain size and pores were generated. These defects caused the permittivity to drop sharply (Fig. 16c).

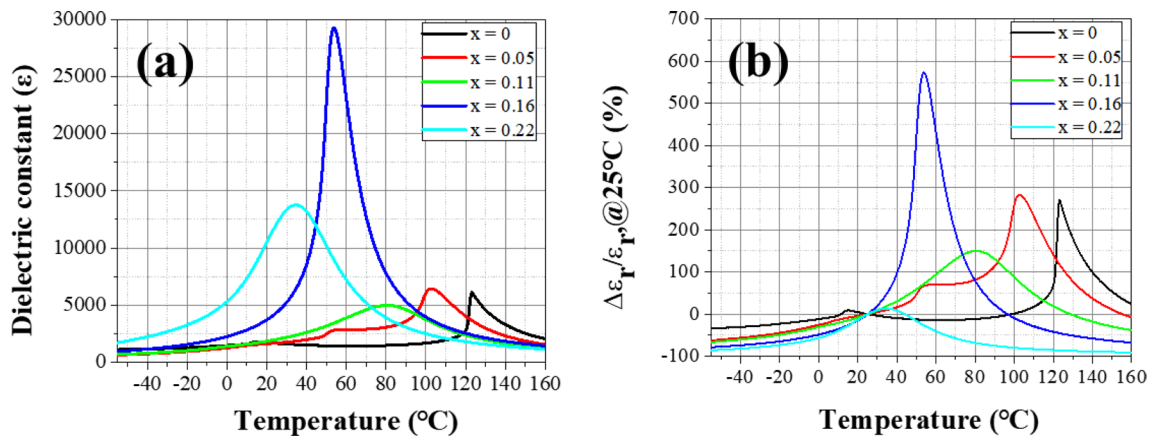


Fig. 12 Analysis results of permittivity changes according to temperature changes in specimens calcinated at 1000 °C and sintered at 1300 °C (a changes in dielectric constant according to temperature changes, b rate of change in dielectric constant according to temperature changes)

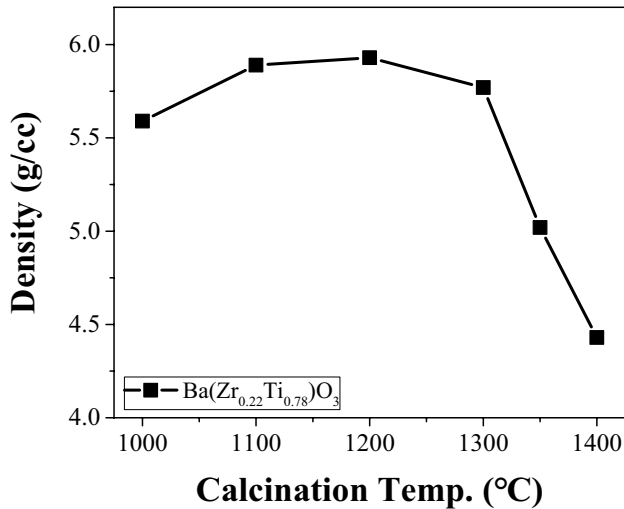


Fig. 13 Sintered density analysis results for Ba(Zr_{0.22}Ti_{0.778})O₃ specimens sintered at 1300 °C after calcination at temperatures of 1000–1400 °C

4 Conclusion

In this study, we attempted to control dielectric properties using Zr, which has a large ionic radius, as a substitute for Ti, the B-site element of BaTiO₃ ferroelectric material. The results showed that when 0.222 mol of Zr was added, high permittivity occurred at room temperature due to changes in lattice volume caused by the DPT phenomenon. In addition, mixing Ba(Zr_{0.222}Ti_{0.778})O₃ and performing synthesis at 1300 °C produced the best results with a permittivity value of 21,700. However, from the synthesis temperature of 1350 °C, the sintering density and dielectric properties decreased rapidly due to coarse grain growth.

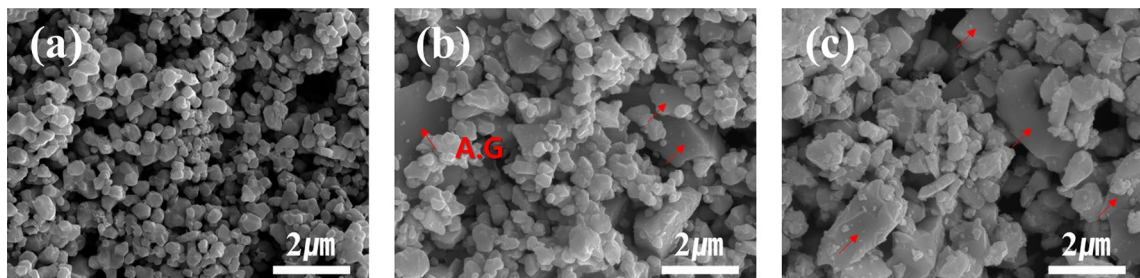


Fig. 14 Results of microstructure analysis of Ba(Zr_{0.222}Ti_{0.778})O₃ powder calcinated at temperatures of 1300–1400 °C (a 1300 °C×4 h, b 1350 °C×4 h, and c 1400 °C×4 h)

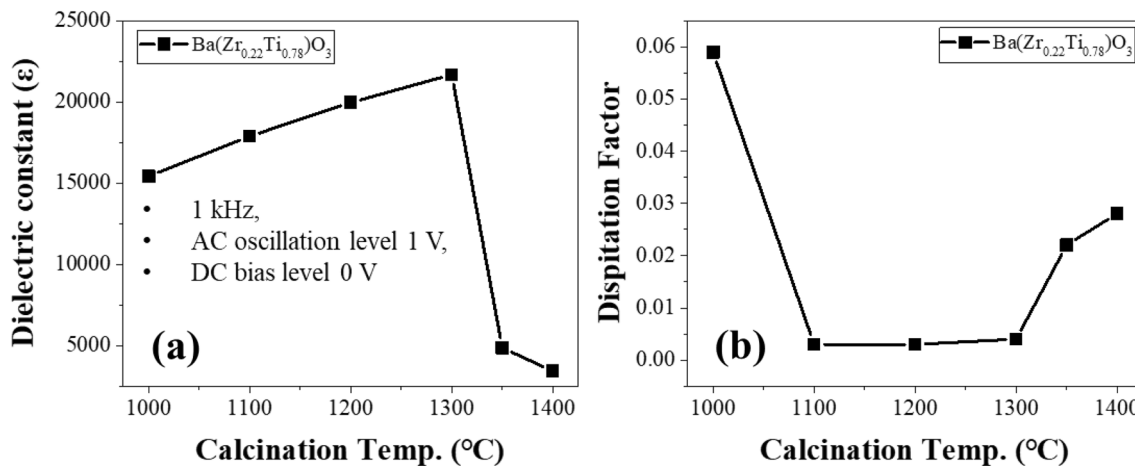


Fig. 15 Results of dielectric properties analysis of $\text{Ba}(\text{Zr}_{0.22}\text{Ti}_{0.778})\text{O}_3$ specimens calcinated at temperatures of 1000–1400 °C and sintered at 1300 °C (a permittivity, b dielectric loss)

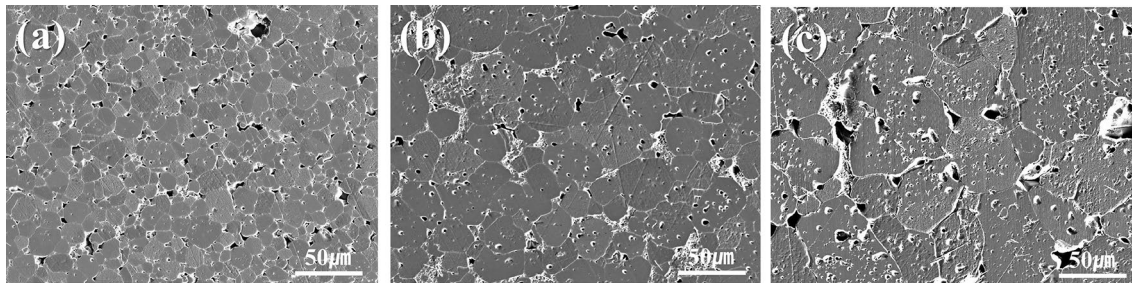


Fig. 16 Microstructure analysis results for fracture surface of $\text{Ba}(\text{Zr}_{0.22}\text{Ti}_{0.778})\text{O}_3$ specimens calcinated at 1200–1350 °C and sintered at 1300 °C (a 1200 °C × 4 h, b 1300 °C × 4 h, and c 1350 °C × 4 h)

Acknowledgements “This study was supported by the materials and parts technology developments (Grant No.20010938), funded by the Ministry of Trade, Industry & Energy (MoTIE, South Korea). This work was supported by Institute for Information & communications Technology Promotion (IITP) grant funded by the Korea government (MSIP) (No.2021-0-00793).”

Funding Ministry of Trade, Industry and Energy, 20010938, Moonhee Choi, Institute for Information and Communications Technology Promotion, 2021-0-00793, Moonhee Choi.

Data availability The data that support the findings of this study are available from the corresponding author upon reasonable request.

Open Access This article is licensed under a Creative Commons Attribution 4.0 International License, which permits use, sharing, adaptation, distribution and reproduction in any medium or format, as long as you give appropriate credit to the original author(s) and the source, provide a link to the Creative Commons licence, and indicate if changes were made. The images or other third party material in this article are included in the article's Creative Commons licence, unless indicated otherwise in a credit line to the material. If material is not included in the article's Creative Commons licence and your intended use is not permitted by statutory regulation or exceeds the permitted use, you will need to obtain permission directly from the copyright holder. To view a copy of this licence, visit <http://creativecommons.org/licenses/by/4.0/>.

References

1. J.Q. Qi et al., Dielectric properties of barium zirconate titanate (BZT) ceramics tailored by different donors for high voltage applications. *Solid State Sci.* **14**, 1520–1524 (2012). <https://doi.org/10.1016/j.solidstatesciences.2012.08.009>
2. Y. Zhang, Y. Li, H. Zhu, Z. Fu, Q. Zhang, Influence of Zr/Ti ratio on the dielectric properties of $\text{BaZr}_x\text{Ti}_{1-x}\text{O}_3$ ceramics for high-voltage capacitor applications. *J. Mater. Sci. Mater. Electron.* **27**, 9572–9576 (2016). <https://doi.org/10.1007/s10854-016-5010-7>
3. M. Deluca et al., Investigation of the composition-dependent properties of $\text{BaTi}_{1-x}\text{Zr}_x\text{O}_3$ ceramics prepared by the modified Pechini method. *J. Eur. Ceram. Soc.* **32**, 3551–3566 (2012). <https://doi.org/10.1016/j.jeurceramsoc.2012.05.007>
4. N. Triamnak, R. Yimnirun, J. Pokorny, D.P. Cann, D.C. Lupascu, Relaxor characteristics of the phase transformation in $(1-x)\text{BaTiO}_3-x\text{Bi}(\text{Zn}_{1/2}\text{Ti}_{1/2})\text{O}_3$ perovskite ceramics. *J. Am. Ceram. Soc.* **96**, 3176–3182 (2013). <https://doi.org/10.1111/jace.12495>
5. W. Li, Z. Xu, R. Chu, P. Fu, G. Zang, Structural and dielectric properties in the $(\text{Ba}_{1-x}\text{Ca}_x)(\text{Ti}_{0.95}\text{Zr}_{0.05})\text{O}_3$ ceramics. *Curr. Appl. Phys.* **12**, 748–751 (2012). <https://doi.org/10.1016/j.cap.2011.10.013>
6. J.Q. Qi et al., Direct synthesis of barium zirconate titanate (BZT) nanoparticles at room temperature and sintering of their ceramics

- at low temperature. *Ceram. Int.* **40**, 2747–2750 (2014). <https://doi.org/10.1016/j.ceramint.2013.10.045>
- 7. J. Panacek. (Texas Instruments, 2018).
 - 8. Z. Liu, A. Ivanco, Z.S. Filipi, Impacts of real-world driving and driver aggressiveness on fuel consumption of 48-V mild hybrid vehicle. *SAE Int. J. Altern. Powertrains.* **5**, 249–258 (2016). <https://doi.org/10.4271/2016-01-1166>
 - 9. D.-W. Lee, J.-H. Lim, D.-I. Lee, H.-S. Youn, A high-power-density active-clamp converter with integrated planar transformer. *Energies* (2022). <https://doi.org/10.3390/en15155609>
 - 10. M. Kuypers, “Application of 48 volt for mild hybrid vehicles and high power loads,” *SAE technical paper, Series* (2014).
 - 11. Y. Tang, T. Wang, Y. He, A switched-capacitor-based active-network converter with high voltage gain. *IEEE Trans. Power Electron.* **29**, 2959–2968 (2014). <https://doi.org/10.1109/tpele.2013.2272639>
 - 12. N.J.A. Sloane, A.S. Hedayat, J. Stufken, *Orthogonal arrays: theory and applications* (Springer, New York, 1999)
 - 13. S.H. Choi et al., Major factors affecting the dielectric properties and reliability of solid stated reacted BaTiO₃ powders for capacitor. *J. Asian Ceram. Soc.* **10**, 713–721 (2022). <https://doi.org/10.1080/21870764.2022.2114671>
 - 14. B.C. Keswani et al., Role of A-site Ca and B-site Zr substitution in BaTiO₃ lead-free compounds: combined experimental and first principles density functional theoretical studies. *J. Appl. Phys.* (2018). <https://doi.org/10.1063/1.5021249>
 - 15. M. Yoon, Y. Park, Effects of A-site Ca and B-site Zr Substitution on the dielectric characteristics and microstructure of BaTiO₃-CaTiO₃ composite. *J. Korean Ceram. Soc.* **40**, 37–45 (2003). <https://doi.org/10.4191/KCERS.2003.40.1.037>
 - 16. J.N. Lin, T.B. Wu, Effects of isovalent substitutions on lattice softening and transition character of BaTiO₃ solid solutions. *J. Appl. Phys.* **68**, 985–993 (1990). <https://doi.org/10.1063/1.346665>
 - 17. J. Su, J. Zhang, Recent development on modification of synthesized barium titanate (BaTiO₃) and polymer/BaTiO₃ dielectric composites. *J. Mater. Sci. Mater. Electron.* **30**, 1957–1975 (2019). <https://doi.org/10.1007/s10854-018-0494-y>
 - 18. S.H. Choi et al., Enhancement of dielectric properties and microstructure control of BaTiO₃ by seed-induced solid-state synthesis. *Ceram. Int.* (2023). <https://doi.org/10.1016/j.ceramint.2023.02.159>
 - 19. Q. Xu, Z. Li, Dielectric and ferroelectric behaviour of Zr-doped BaTiO₃ perovskites. *Process. Appl. Ceram.* **14**, 188–194 (2020). <https://doi.org/10.2298/PAC200318X>
 - 20. E. Chandrakala, J. Paul Praveen, B.K. Hazra, D. Das, Effect of sintering temperature on structural, dielectric, piezoelectric and ferroelectric properties of sol-gel derived BZT-BCT ceramics. *Ceram. Int.* **42**, 4964–4977 (2016). <https://doi.org/10.1016/j.ceramint.2015.12.009>
 - 21. D.S. Kim, J.S. Kim, C.I. Cheon, Effects of sintering atmosphere on piezoelectric properties of 0.75BF-0.25BT ceramic. *J. Korean Ceram. Soc.* **53**, 162–166 (2016). <https://doi.org/10.4191/kcers.2016.53.2.162>
 - 22. S.K. Sourav, S.K. Parida, R.N.P. Choudhary, U. Prasad, Structural, microstructural, dielectric, transport, and optical properties of modified bismuth ferrite. *J. Korean Ceram. Soc.* **60**, 687–701 (2023). <https://doi.org/10.1007/s43207-023-00294-5>
 - 23. M. Choi, S. Cho, Y. Song, S. Park, Y. Kim, Simultaneous enhancement in coercivity and remanence of Nd₂Fe₁₄B permanent magnet by grain boundary diffusion process using NdHx. *Curr. Appl. Phys.* **15**, 461–467 (2015). <https://doi.org/10.1016/j.cap.2015.01.025>
 - 24. X. Zang et al., Dielectric properties and thermal conductivity of Si₃N₄-SiC composite ceramics. *J. Korean Ceram. Soc.* **59**, 903–908 (2022). <https://doi.org/10.1007/s43207-022-00232-x>
 - 25. H.A. Alburaih et al., The electrical, dielectric and magnetic effect of MgFe₂O₄-polypyrrrole and its composites. *J. Korean Ceram. Soc.* **60**, 357–363 (2022). <https://doi.org/10.1007/s43207-022-00270-5>
 - 26. B. D. Cullity, *Magnetic Materials*; pp. 378, ITC, Seoul, 2003.
 - 27. E.G. Villora, K. Shimamura, T. Ujiie, K. Aoki, Electrical conductivity and lattice expansion of β -Ga₂O₃ below room temperature. *Appl. Phys. Lett.* (2008). <https://doi.org/10.1063/1.2910770>

Publisher's Note Springer Nature remains neutral with regard to jurisdictional claims in published maps and institutional affiliations.